Structure of Reduced DsbA from *Escherichia coli* in Solution[†,‡]

Horst Joachim Schirra,[§,||] Christian Renner,[§] Michael Czisch,[§,⊥] Martina Huber-Wunderlich,[||] Tad A. Holak,*[,§] and Rudi Glockshuber*[,||]

Max-Planck-Institut für Biochemie, Am Klopferspitz 18a, D-82152 Martinsried, Germany, and Institut für Molekularbiologie und Biophysik, Eidgenössische Technische Hochschule Hönggerberg, CH-8093 Zürich, Switzerland

Received January 20, 1998

ABSTRACT: The three-dimensional structure of reduced DsbA from *Escherichia coli* in aqueous solution has been determined by nuclear magnetic resonance (NMR) spectroscopy and is compared with the crystal structure of oxidized DsbA [Guddat, L. W., Bardwell, J. C. A., Zander, T., and Martin, J. L. (1997) *Protein Sci. 6*, 1148−1156]. DsbA is a monomeric 21 kDa protein which consists of 189 residues and is required for disulfide bond formation in the periplasm of *E. coli*. On the basis of sequence-specific ^{1}H NMR assignments, 1664 nuclear Overhauser enhancement distance constraints, 118 hydrogen bond distance constraints, and 293 dihedral angle constraints were obtained as the input for the structure calculations by simulated annealing with the program X-PLOR. The enzyme is made up of two domains. The catalytic domain has a thioredoxin-like fold with a five-stranded β-sheet and three α-helices, and the second domain consists of four α-helices and is inserted into the thioredoxin motif. The active site between Cys30 and Cys33 is located at the N terminus of the first α-helix in the thioredoxin-like domain. The solution structure of reduced DsbA is rather similar to the crystal structure of the oxidized enzyme but exhibits a different relative orientation of both domains. In addition, the conformations of the active site and a loop between strand β5 and helix α7 are slightly different. These structural differences may reflect important functional requirements in the reaction cycle of DsbA as they appear to facilitate the release of oxidized polypeptides from reduced DsbA. The extremely low pK_a value of the nucleophilic active site thiol of Cys30 in reduced DsbA is most likely caused by its interactions with the dipole of the active site helix and the side chain of His32, as no other charged residues are located next to the sulfur atom of Cys30 in the solution structure.

The formation of disulfide bonds in secretory proteins is often a slow and rate-limiting step during protein folding and is catalyzed by enzymes in vivo (*1*). In the periplasmic space of *Escherichia coli*, the thiol−disulfide oxidoreductase DsbA is required for the introduction of disulfide bridges into folding polypeptides (*2*, *3*). DsbA possesses a catalytic disulfide bond and randomly oxidizes reduced, unfolded proteins in an extremely rapid disulfide exchange reaction (*4*−*6*). Reduced DsbA is then reoxidized by disulfide interchange with DsbB, a protein from the inner membrane of *E. coli* (*7*−*11*).

DsbA is a soluble monomer of 189 amino acids (*2*). The crystal structure of oxidized DsbA has been determined to 1.7 Å resolution and has revealed that DsbA consists of two domains (*12*, *13*). The catalytic domain (residues 1−62 and 139−189) has the thioredoxin fold, the common motif of all thiol−disulfide oxidoreductases, although there is only 10% sequence identity between the catalytic domain of DsbA and *E. coli* thioredoxin (*12*, *14*). The second domain (residues 63−138) exclusively consists of α-helices and is inserted into the thioredoxin motif. The active site of DsbA (Cys30-Pro31-His32-Cys33) is located at the amino-terminal end of the first α-helix in the thioredoxin-like domain. While the thiol of Cys30 is solvent-exposed and acts as a nucleophile in reduced DsbA, the thiol of Cys33 is buried in the interior of the protein (*13*, *15*−*17*).

Despite the structural similarities with other thiol−disulfide oxidoreductases such as thioredoxin, glutaredoxin, thioltransferase, and protein disulfide isomerase (*14*, *18*, *19*), DsbA shows remarkable biophysical properties which make it unique in this protein family. The enzyme is the most oxidizing thiol−disulfide oxidoreductase with a redox potential (E_0') of −122 mV (*20*, *21*), compared to a value of −270 mV for the most reducing member of the protein family, thioredoxin (*22*, *23*). Reduced DsbA is more stable than the oxidized form (*24*), and the enzyme shows very high reaction rates with thiol substrates even at low pH (*4*, *6*, *15*, *25*). Thus, DsbA is an ideal oxidant for reduced polypeptides in the bacterial periplasm. The oxidative force of DsbA, its destabilizing disulfide bond, and its fast disulfide exchange reactions can, at least qualitatively, be explained by the extremely low pK_a of 3.5 of the nucleophilic thiol of Cys30 (*26*). In addition, DsbA has been shown to interact specifically with reduced, unfolded polypeptides and appears

† This work was supported by grants from the Deutsche Forschungsgemeinschaft (Sonderforschungsbereich 533 der Ludwig-Maximilians-Universität München), the ETH Zürich, and the Fonds der Chemischen Industrie.

‡ The coordinates of the 20 best conformers and the energy-minimized mean structure of reduced DsbA have been deposited in the Brookhaven Protein Data Bank (accession codes 1a24 and 1a23).

* Corresponding authors. For a proof query contact Rudi Glockshuber. Phone: +41 (1) 633-6819. Fax: +41 (1) 633-1036.

§ Max-Planck-Institut für Biochemie.

|| Eidgenössische Technische Hochschule Hönggerberg.

⊥ Present address: Bijvoet Center for Biomolecular Research, Utrecht University, Padualaan 8, NL-3584 CH Utrecht, The Netherlands.

S0006-2960(98)00136-6 CCC: $15.00
Published on Web 04/16/1998

to possess a peptide binding site (*4*−*6*, *25*, *27*) which has been attributed to a hydrophobic region in the vicinity of the active site disulfide (*13*). However, the molecular basis for the low pK_a value of Cys30 in reduced DsbA is not yet completely understood because the structure of reduced DsbA has not been determined so far. It is generally assumed that interactions between the Cys30 thiolate and the dipole of the active site helix (*26*, *28*−*30*) as well as the residues of the dipeptide between the two active site cysteines (*21*, *23*, *31*−*35*) are mainly responsible for the pK_a of DsbA's nucleophilic cysteine. Additional mechanisms have been discussed for DsbA and the homologous protein thioredoxin, such as a charged hydrogen bond between the thiolate and the thiol or the amide hydrogen of the buried cysteine (*29*, *36*−*39*) or interactions with charged residues in the vicinity of the active site (*40*).

Apart from this, a structural comparison of oxidized and reduced DsbA should shed light on the physicochemical properties of the enzyme. It has for example been speculated that both domains of DsbA could move relative to each other when the protein is reduced and that such a movement could be of functional significance (*13*, *41*). On the other hand, the structural comparison of the oxidized and reduced forms of human and *E. coli* thioredoxin and *E. coli* glutaredoxin revealed only slight local differences (*29*, *37*, *39*, *42*−*47*). Overall, knowledge of the three-dimensional structure of reduced DsbA is required for understanding the extraordinary properties of this enzyme at a molecular level.

Here we report the determination of the three-dimensional structure of reduced DsbA at pH 3.7 and 300 K in solution by NMR[1] spectroscopy. We compare the structure of reduced DsbA with the crystal structure of the oxidized protein (*13*) and discuss the structural differences between both redox forms with respect to their functional significance.

MATERIALS AND METHODS

Materials. 1,4-Dithio-DL-threitol (DTT), amino acids, ampicillin, and polymyxin B sulfate were purchased from Sigma (Deisenhofen, Germany). Isopropyl β-D-thiogalactoside (IPTG) was from AGS GmbH (Heidelberg, Germany). [^{15}N]Ammonium chloride and [^{13}C]glucose were obtained from Campro Scientific (Emmerich, Germany). D_2O was from Cambridge Isotope Laboratories (Cambridge, Great Britain). DE52 cellulose was purchased from Whatman (Maidstone, United Kingdom) and phenyl Sepharose from Pharmacia (Uppsala, Sweden). All other chemicals were from Merck (Darmstadt, Germany) or Fluka (Buchs, Switzerland) and of the highest purity available.

Sample Preparation. For the preparation of uniformly ^{15}N-labeled DsbA, the protein was overproduced in *E. coli* BL21 cells (*48*) harboring the plasmid pRBI-PDI-T7 (*49*). The cells were grown at 26 °C in a M9 minimal medium (*50*) containing ampicillin (100 μg/mL) and 1 g/L $^{15}NH_4Cl$ as the sole nitrogen source. Selective ^{15}N labeling of glycines and serines was achieved with M9 minimal medium that contained 1 g/L $^{15}NH_4Cl$, 1 g/L [^{15}N]glycine, and the residual unlabeled amino acids, except for serine (*51*).

For preparation of uniformly ^{15}N and ^{13}C doubly labeled DsbA, cells were grown in a minimal medium (*52*) that contained 1 g/L $^{15}NH_4Cl$ and 1 g/L [^{13}C]glucose as sole sources of nitrogen and carbon.

Purification of DsbA by anion exchange chromatography on DE52 cellulose and hydrophobic chromatography on phenyl Separose was performed as previously described (*20*). The DsbA concentration was determined by its absorbance at 280 nm (*20*). The purified protein was shown to be fully oxidized. Purified DsbA was dialyzed against 20 mM H_3PO_4/NaOH, at pH 3.7 and concentrated to 1−3.5 mM. Finally, the protein was reduced in the NMR tube by a 5-fold molar excess of d_{10}-DTT and kept under nitrogen. The samples contained either 5% D_2O (v/v) ("samples in H_2O") or 100% D_2O in a volume of 500 μL.

NMR Spectroscopy. (1) General Conditions. Spectra were recorded at 300 K on Bruker AMX600, DRX600, and DMX750 spectrometers with triple-resonance self-shielded *z*-gradient 5 mm probes. Quadrature detection in the indirect dimensions was achieved using the TPPI (*53*) or the States−TPPI method (*54*). Sweep widths were 14.17 ppm for ^{1}H, 34.53 ppm for ^{15}N, and 75.3 ppm for ^{13}C. Carriers were positioned at 4.73 ppm (^{1}H), 119.24 ppm (^{15}N), and 34.11 ppm (^{13}C) for the respective nuclei. NOESY experiments were recorded with a pulse sequence in which the last 90° pulse was either substituted by a jump−return sequence (*55*) or followed by a 3−9−19 WATERGATE sequence (*56*) to suppress the water resonance. TOCSY experiments used the MLEV16 sequence (*57*) for isotropic mixing and included a presaturation of the water resonance (*58*) for measurements in water. Essentially the same pulse sequences were used for measurements in D_2O, with the exception that no water suppression was necessary.

(2) Data Acquisition. The following spectra were recorded on the ^{15}N-labeled sample: ^{15}N-NOESY−HSQC (*59*) with 180 × 68 × 1K data points in f_1, f_2, and f_3, respectively, and a mixing time of 110 ms and ^{15}N-TOCSY−HSQC (*60*) with 176 × 54 × 1K data points and a spin-lock period of 61.5 ms. Additionally, a ^{15}N-HSQC spectrum (*61*) was recorded with 108 × 1K* data points in f_1 and f_2, respectively (* denotes complex data points). For identification of glycine and serine residues, a ^{15}N-HSQC spectrum with a size of 64 × 1K* data points was recorded on the Gly and Ser ^{15}N-labeled sample. The following spectra were recorded on the uniformly ^{15}N and ^{13}C doubly labeled sample in 5% D_2O: ct-HNCA (*62*), HN(CA)CO (*63*), ct-HNCO (*62*, *64*), CBCANH (*65*), CBCA(CO)NH (*64*), HBHA(CBCACO)NH (*66*), HBHA(CBCA)NH (*67*), HNHA (*68*), HNHB (*69*), ct-HCACO (*70*), and HCCH-TOCSY (*71*) (114* × 49* × 512* data points with an 18 ms mixing time for the HCCH-TOCSY (a DIPSI-3y sequence (*72*) was used for isotropic mixing)); HCCH-TOCSY (180* × 70* × 1K* data points with a 16 ms spin-lock time); and ^{13}C-NOESY−HSQC (*73*) (172 × 124 × 512* data points with a mixing time of 100 ms). In addition, a ^{13}C-NOESY−HSQC spectrum (216* ×

[1] Abbreviations: 2D, two-dimensional; 3D, three-dimensional; NMR, nuclear magnetic resonance; NOE, nuclear Overhauser effect; NOESY, NOE spectroscopy; TOCSY, total correlation spectroscopy; CBCANH, intra- and interresidue $^1H^N$, ^{15}N, $^{13}C^\beta$, and $^{13}C^\alpha$ correlation; CBCA(CO)NH, interresidue $^1H^N$, ^{15}N, $^{13}C^\beta$, and $^{13}C^\alpha$ correlation; ct, constant time; HBHA(CBCA)NH, intra- and interresidue $^1H^N$, ^{15}N, $^1H^\beta$, and $^1H^\alpha$ correlation; HBHA(CBCACO)NH, interresidue $^1H^N$, ^{15}N, $^1H^\beta$, and $^1H^\alpha$ correlation; HCACO, intraresidue $^1H^\alpha$, $^{13}C^\alpha$, and $^{13}C'$ correlation; HNCA, intra- and interresidue $^1H^N$, ^{15}N, and $^{13}C^\alpha$ correlation; HN(CA)CO, intra- and interresidue $^1H^N$, ^{15}N, and ^{13}C' correlation; HNCO, interresidue $^1H^N$, ^{15}N, and ^{13}C' correlation; HNHA, intraresidue $^1H^N$, ^{15}N, and $^1H^\alpha$ correlation; HSQC, heteronuclear single-quantum correlation; rmsd, root-mean-square deviation; SA, simulated annealing.

64* × 1K* data points) with a 120 ms mixing time was recorded on the doubly labeled sample dissolved in D_2O.

A homonuclear 2D NOESY spectrum (*74*) with a mixing time of 60 ms (960 × 2K* data points) and a 2D TOCSY spectrum with a spin-lock period of 40 ms (512 × 2K* data points) were recorded on an unlabeled DsbA sample in H_2O. In addition, a 2D NOESY spectrum with a mixing time of 40 ms (1050 × 2K* data points) was recorded on an unlabeled sample in 100% D_2O. An amide proton exchange experiment was performed after lyophilization of ^{15}N-labeled, reduced DsbA in 20 mM H_3PO_4/NaOH at pH 3.7 and dissolving the protein in D_2O. Within 24 h, 10 ^{15}N-HSQC spectra (128 × 1K* data points) were recorded. Additional ^{15}N-HSQC spectra were recorded after 1, 2, and 8 weeks.

(3) Processing of Data. All spectra were processed and analyzed with the in-house written programs CCNMR and GLXCC (*75*). Zero filling or linear prediction was used to prolong the number of time domain points in f_1 and f_2. Before Fourier transformation, the data were multiplied with an appropriate window function (Gauss window or shifted squared sine).

Chemical Shift Assignment. Unlabeled, uniformly ^{15}N-labeled, ^{15}N and ^{13}C doubly labeled, and selectively glycine and serine ^{15}N-labeled DsbA samples were used for the assignment of proton resonances and structure determination of the reduced protein. Assignments of the NMR spectra of DsbA were made using heteronuclear triple-resonance NMR methods (*76*). The assignment was carried out both manually and by using the program ALFA (*77*) which was modified for the assignment of triple-resonance spectra. Backbone C^α and C^β resonances were assigned with HNCA, CBCA(CO)NH, and CBCANH spectra. HNCO and HN(CA)CO were used to assign the C′ resonances. H^α and H^β resonances were assigned using HBHA(CBCACO)NH and HBHA(CBCA)NH. The resonance signals of the amino acid side chains were assigned with ^{13}C- and ^{15}N-NOESY−HSQC spectra, a HCCH-TOCSY spectrum, and a 2D NOESY spectrum, all measured in 5% D_2O, and with a ^{13}C-NOESY−HSQC spectrum in 100% D_2O. The signals of the aromatic ring systems were assigned with the 2D NOESY and TOCSY spectra.

Stereospecific Assignments and Coupling Constants. Stereospecific assignments of $C^\beta H$ protons and methyl groups of valines and leucines were obtained using procedures described by Wagner et al. (*78*) and Hyberts et al. (*79*). The assignment of $C^\beta H$ protons was confirmed by data from the HNHB spectrum (*69*). $^3J_{H^\alpha HN}$ coupling constants were measured from a 3D ^{15}N-separated H^N-H^α correlation spectrum HNHA (*68*) which yielded the coupling constants from the ratio of the H^N-H^α cross-peak to the H^N-H^N diagonal peak intensity.

Interproton Distance Constraints. Interproton distances were derived from the following spectra: 3D ^{15}N-NOESY−HSQC in 5% D_2O, 3D ^{13}C-NOESY−HSQC in 100% D_2O, 2D NOESY in 5% D_2O, and 2D NOESY in 100% D_2O with mixing times of 100, 200, 60, and 40 ms, respectively. The intensities of the NOE cross-signals were converted into distance constraints as described previously (*80*). The distance bounds of the distance constraints were set to $d \pm 0.5$ Å for distance constraints between 2.2 and 3.5 Å and to $d \pm 0.8$ Å for distance constraints between 3.6 and 4.5 Å. All protons were explicitly defined in the structure calculations. However, in some cases, additional terms were added to the upper bounds corresponding to the pseudoatom correction introduced by Wüthrich (*81*).

Torsion Angle and Hydrogen Bond Constraints. The distance constraints were supplemented with 131 backbone ϕ torsion angle constraints derived from the $^3J_{H^\alpha HN}$ coupling constant data and with 5 ψ angles for the trans peptide bond of the Xaa-Pro residues (*81*). The ϕ constraints were introduced in two stages. At the initial stage of structure calculation, only those ϕ constraints were used which corresponded to $^3J_{H^\alpha HN}$ coupling constants larger than 8 Hz ($\phi = -120 \pm 40°$) (*81*). The other ϕ constraints and the 94 additional ψ constraints were introduced at a late stage of the refinement procedure (see below). Sixty χ_1 and 5 χ_2 torsion angle constraints were derived from stereochemical assignment of side chain protons. The minimum range employed was ±50° for ψ and ±20° for the other torsion angles. Hydrogen bonds were identified on the basis of NOE patterns and deuterium exchange data during secondary structure determination and later during examination of the calculated 3D structures (*80*, *81*).

Structure Calculations and Refinement. A total of 20 structures were calculated with the program X-PLOR 3.851 (*82*) using a simulated annealing protocol that starts from random coordinates or an extended conformation followed by several rounds of short SA refinement. The basic protocol used with minor modifications for the calculations has been described previously (*80*). For the final refinement, the NOE tables were supplemented with 118 constraints for 59 hydrogen bonds. In addition, the NOE tables were supplemented at this stage with the ϕ constraints derived from the $^3J_{H^\alpha HN}$ constants of <8 Hz (80). The ϕ constraints were introduced for residues whose ϕ values were close (within ±20°) to the mean value in structures calculated without dihedral constraints and which fulfilled the Karplus equation (*81*).

RESULTS

Sequence-Specific Assignment of the ^{1}H, ^{15}N, and ^{13}C Resonances and Identification of Cis Prolines. The NMR spectra of reduced DsbA were recorded at pH 3.7 and 300 K. Data collected at pH 4.0 served for confirmation of assignments. The NMR spectra of DsbA were assigned with triple-resonance spectra and other 3D NMR methods (*76*, *81*). As an example of the quality of the spectra, the ^{15}N-HSQC spectrum of reduced DsbA is shown in Figure 1. Proton resonances of all backbone atoms were assigned with the exception of the amide protons of Ala1 and His32. The resonances of most of the aliphatic (84%) and aromatic (70%) side chain protons could also be unambiguously assigned. The NH_2 protons of all asparagine and glutamine residues could be assigned with the exception of the NH_2 groups of Gln8, Gln137, Gln146, Asn156, Gln160, and Gln177, for which too few connectivities could be observed in the spectra.

The complete spin systems of Pro15 and Pro51 could be identified. Both are in the trans conformation because strong $H^\delta(i)$Pro$-H^\alpha(i-1)$ NOE signals were observed in the NOESY spectra (*81*). The spin systems of Pro20, Pro31, Pro151, and Pro163 could not be assigned completely, but there were enough data to prove that Pro20, Pro31, and Pro163 are also in the trans conformation because both the

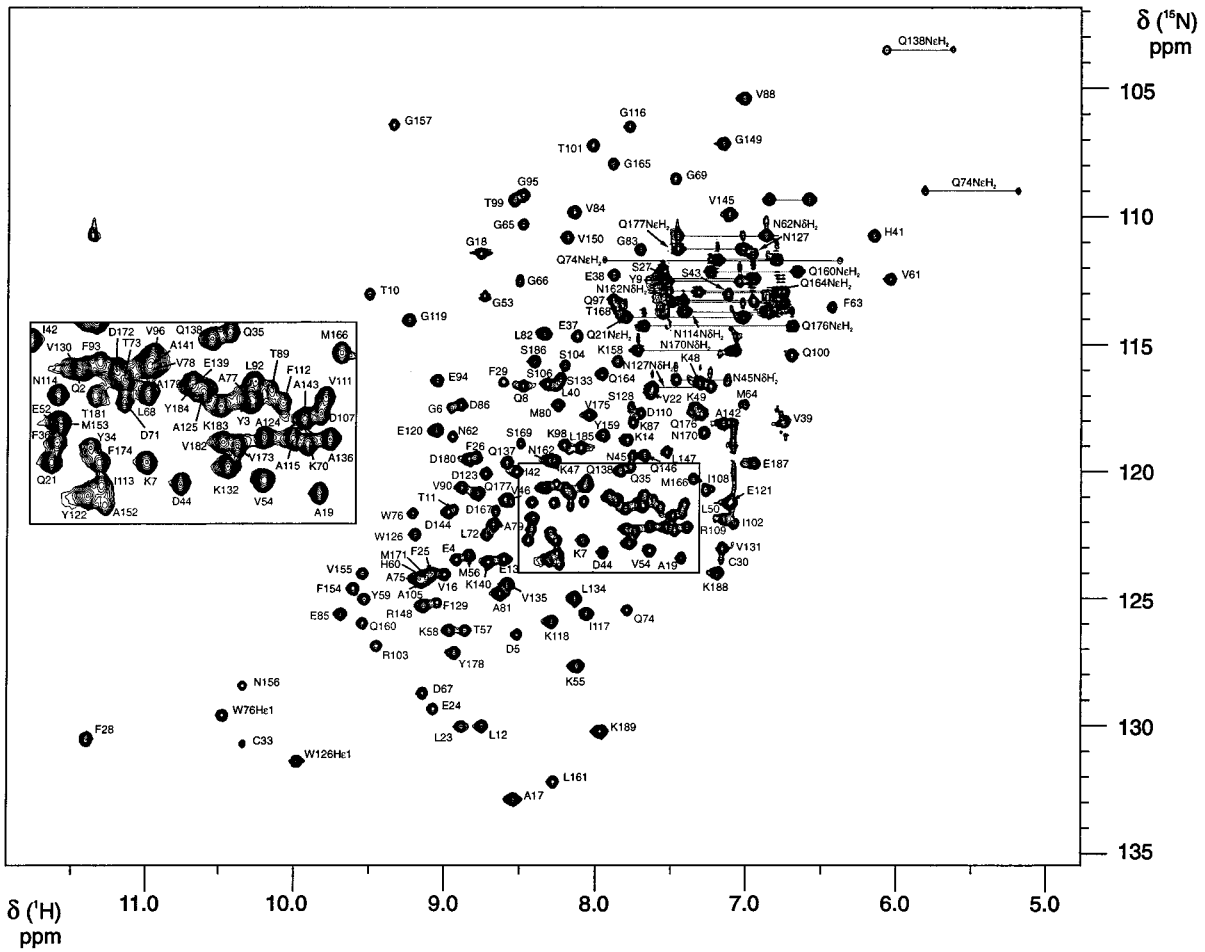

FIGURE 1: HSQC spectrum of uniformly ^{15}N-labeled reduced DsbA at 300 K and pH 3.7. The assignment of each resonance is indicated next to the corresponding signal. A region with strong signal overlap (marked with a rectangle) is magnified at the left side of the figure. Signals connected by horizontal lines correspond to side chain NH_2 groups of asparagine and glutamine.

$H^N(i+1)-H^\alpha(i)$Pro and $H^\delta(i)$Pro$-H^\alpha(i-1)$ connectivities could be observed for these residues. Pro151 is in the cis conformation since a strong cross-signal between H^α(Pro151) and H^α(Val150) could be observed which is diagnostic for the cis conformation (*81*). Data for Pro91 were ambiguous as the cross-signal between H^α(Val90) and H^δ(Pro91) could not certainly be identified. The intensity of the H^N(Leu92)$-H^\alpha$(Pro91) cross-signal was markedly lower than that of equivalent cross-signals of other trans prolines. However, the diagnostic H^α(Val90)$-H^\alpha$(Pro91) cross-signal could not be identified due to spectral overlap. Therefore, the conformation of Pro91 was not constrained in the structure calculations which resulted in a trans conformation for Pro91 in all structures calculated with X-PLOR.

Secondary Structure and Domains in Reduced DsbA. Figure 2 summarizes sequential and medium-range NOEs observed in the spectra of reduced DsbA. These NOEs are the basis for the determination of the protein's secondary structure. Many sequential $H^N(i)-H^N(i+1)$, $H^N(i)-H^N(i+2)$, and $H^\alpha(i)-H^N(i+3)$ cross-signals, typical for α-helices, were found in the spectra (Figure 2). β-Strands were identified by the presence of strong sequential $H^\alpha(i)-H^N(i+1)$ and weak intraresidual $H^\alpha(i)-H^N(i)$ cross-signals and by interstrand $H^N(i)-H^N(j)$, $H^N(i)-H^\alpha(j)$ and $H^\alpha(i)-H^\alpha(j)$ NOEs (*81*).

Seven α-helices were identified between residues 31−37, 42−48, 68−82, 85−97, 105−114, 119−127, 130−144, and 171−185, and five β-strands were found between residues 9−11, 22−25, 56−59, 152−155, and 159−161. Interstrand $H^N(i)-H^N(j)$, $H^N(i)-H^\alpha(j)$, and $H^\alpha(i)-H^\alpha(j)$ NOEs were observed in all five strands, allowing the identification of the corresponding hydrogen bonds between adjacent strands (*81*). The five β-strands form the central β-sheet of the thioredoxin-like domain with the topology 1a5a4a2p3, where a denotes antiparallel and p parallel connections between strands. The termini of the secondary structure elements are generally the same as those for the crystal structure of oxidized DsbA (*13*) with small deviations of one or two residues. Only strand β2 and the C-terminal helix α7 were three residues shorter.

The thioredoxin-like domain of DsbA is formed by the five-stranded β-sheet and by helices α1, α1′, and α7 and parts of helix α6. The long helix α6 spans both domains of the protein. The helical domain of DsbA which is inserted into the thioredoxin fold is formed by helices α3, α4, and α5 and parts of helix α6. Overall, the helical domain is formed by residues 63−138.

Tertiary Structure. The three-dimensional structure of reduced DsbA was calculated from 1782 approximate interresidue distance constraints. Intraresidue constraints were used for stereospecific assignments of protons and methyl groups, but these constraints were not used in the structure calculations. The global fold of the polypeptide chain is uniquely defined due to the large number of

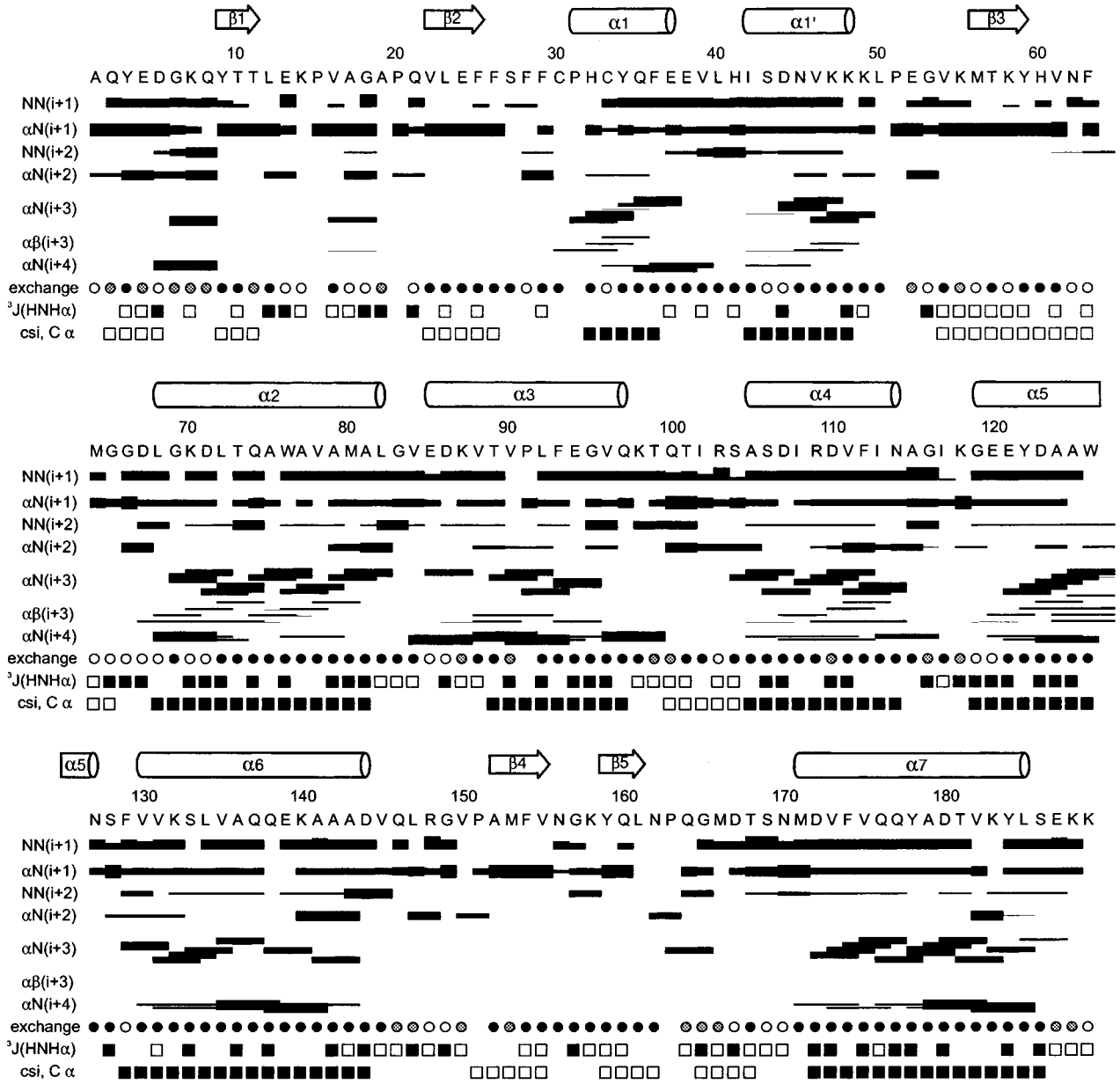

FIGURE 2: Amino acid sequence of DsbA and survey of NMR data used to identify regular secondary structure. The sequential and medium-range NOEs ($|i - j| < 5$), classified as weak, medium, strong, and very strong, are represented by the heights of bars. Medium-range NOEs are indicated by lines connecting the two residues related by the NOE. The $C^{\alpha}H(H^{N})(i)-C^{\delta}H(i+1)$ NOEs of Pro residues are shown along the same line as the $C^{\alpha}H(H^{N})(i)-H^{N}(i+1)$ connectivities. Open circles below the amino acid sequence indicate the positions of amide protons that exchange within 17 min after dissolving a lyophilized protein sample in D_2O at 300 K and pD 3.7. Amide protons still visible after 12 and 24 h are indicated by gray and black circles, respectively. The values of the $^3J_{H^{\alpha}HN}$ coupling constants (in hertz) are indicated by filled ($J < 7$ Hz) and open ($J > 7$ Hz) squares. The chemical shift index (*90*) is also indicated below the sequence with filled and open squares designating α-helices and *β*-sheets, respectively. The arrows and helices at the top of the figure indicate the position of regular secondary structure elements in reduced DsbA as determined from all NMR data.

nonredundant NOEs (Figure 3A,B). The average number of interresidue constraints per residue is 9.4 which results from the extensive assignment of cross-signals in the NOESY spectra.

A total of 20 structures were calculated by a simulated annealing method with the program X-PLOR 3.851 (*82*). All structures satisfy the experimental constraints with small deviations from idealized covalent geometry (Table 1). Figure 3B shows the ensemble of 20 three-dimensional structures of reduced DsbA. The average rmsd from the mean structure for heavy atoms in the well-defined core of DsbA (residues 3−185, except for residues 47−53, 64−66, 97−99, and 163−173) was 0.63 Å for the backbone atoms and 0.96 Å for all atoms (Figure 4). The average rmsd from the mean structure for the ϕ and ψ angles was 19 and 15°, respectively. Larger rmsd values (about 2 Å for the backbone atoms and about 36° for the ϕ backbone torsion angles) were observed for the N and C termini of the protein (residues 1, 2, and 186−189).

Figure 4 shows that the backbone of reduced DsbA is well defined with the exception of residues 47−53, 64−66, 97−99, and 163−173 and both termini of the protein. In general, the conformations of the side chains are also well defined. Most of the backbone torsion angles for non-glycine residues lie within allowed regions of the Ramachandran plot. The few non-glycine residues outside these regions (Tyr3, Asp5,

Table 1: Parameters Characterizing the Structure Determination of Reduced DsbA in Solution at pH 3.7 and 300 K[a]

parameter	⟨SA⟩
deviations from idealized geometry	
bond lengths (Å) (2984)	0.003 ± 0.000
angles (deg) (5397)	0.572 ± 0.006
impropers (deg) (1564)	0.383 ± 0.008
energies (kcal mol^{-1})	
E_{NOE}	154.5 ± 9.4
E_{tor}	3.5 ± 0.6
E_{vdW}	27.9 ± 2.2
number of residual constraint violations for all distance constraints	
0.3 Å ≤ rmsd ≤ 0.4 Å	6.0 ± 1.0
0.4 Å < rmsd ≤ 0.5 Å	0.1 ± 0.2
>0.5 Å	0
rmsd from experimental distance constraints (Å)	
all (1782)	0.041 ± 0.001
sequential (664)	0.054 ± 0.002
medium-range (483)	0.040 ± 0.002
long-range (517)	0.022 ± 0.006
H-bond distances (118)	0.028 ± 0.002

[a] ⟨SA⟩ represents the ensemble of the 20 final structures. The number of bonds, angles, and impropers is given in parentheses. Force constants used to calculate energy terms are the same as reported previously (*80*). The rmsd of the interproton distance constraints was calculated as described in Holak et al. (*80*). The number of distance constraints is given in parentheses. Besides the 1782 distance constraints, 293 dihedral angle constraints were used as input data for the structure calculations.

Thr99, Leu147, and Gln146) are located at the structural interfaces of helices and sheets and connecting loops.

Figure 3B shows an ensemble of the three-dimensional structures of reduced DsbA, calculated from 1782 approximate interproton distance constraints. All structures are basically similar to the crystal structure of the oxidized protein (Figure 5). Local differences are observed in loop regions at the surface of the protein. Especially the loop between residues 162 and 171, which is located between the end of strand β5 and the beginning of helix α7, has different conformations in the ensemble of NMR models compared to the X-ray models. The exact conformation in the solution structure could not be determined as only a few medium- and long-range NOE signals could be identified in the loop, but the energy-minimized mean solution structure which approximates the average structure over time is clearly different (Figure 6). In general, the backbone of the loop runs in the plane which is defined by strand β5 and helix α7. However, in the crystal structure of oxidized DsbA, a part of the loop comprising residues 163−169 is bent and lies below this plane with an angle of roughly 90° between this part of the loop and the β5−α7 reference plane. In the solution structure of reduced DsbA, the part of the loop which is folded "down" in the crystal structure of oxidized DsbA is folded upward into the β5−α7 plane with residues Pro163 and Ser169 being the "hinge points" of this conformational difference so that the backbone runs more or less within the plane from the end of strand β5 to the beginning of the helix α7.

Domain Association in Reduced DsbA. A small but clear difference in the relative positions of the two domains was detected in the refined crystal structure of oxidized DsbA between the two DsbA monomers in the asymmetric unit (*13*). We performed a detailed analysis of the relative domain orientations in the solution structures of reduced DsbA and compared them with those in the two monomers in the crystal structure of oxidized DsbA. First, the energy-minimized mean solution structure of reduced DsbA was compared with the refined crystal structure of oxidized DsbA. Superposition of the structures of reduced and oxidized DsbA (using the C^α atoms of residues 9−11, 22−25, 31−37, 42−48, 56−59, 68−82, 85−97, 105−114, 119−126, 152−155, 159−161, and 171−185) yields an rmsd of 1.86 Å for the C^α atoms. When the thioredoxin-like domain of reduced DsbA (C^α atoms of residues 9−11, 22−25, 31−37, 42−48, 56−59, 152−155, 159−161, and 171−185) is superimposed onto that of oxidized DsbA, the rmsd in C^α position drops to 1.20 Å. Similarly, the helical domains (C^α atoms of residues 68−82, 85−97, 105−114, and 119−126) can be superimposed with an rmsd of 1.22 Å for the C^α positions. However, when the helical domain of reduced DsbA is first aligned with that of the oxidized protein, significant movements are necessary for a subsequent superposition of their thioredoxin-like domains, corresponding to different orientations of the two domains (Figure 7). For reduced DsbA and monomer A of oxidized DsbA, these movements involve a translation of 1.76, −12.5, and 11.8 Å along the *x*, *y*, and *z* axes, respectively, of the coordinate frame and a rotation κ of 20.2° about a rotation axis defined by spherical polar coordinates of $\psi = 84.2°$ (inclination against the *y* axis) and $\phi = 6.0°$ (azimuth, angle between the *x* axis and projection of the rotation axis onto the *x*−*z* plane). If the same fitting procedure for reduced DsbA is applied using monomer B from the crystal structure of oxidized DsbA, the corresponding values are translation of $x = 3.5$ Å, $y = -12.2$ Å, and $z = 10.5$ Å and a rotation of $\kappa = 18.9°$ about an axis with $\psi = 78.2°$ and $\phi = 9.3°$. Comparison of monomer A and B of the crystal structure of oxidized DsbA yields the following values: translation of $x = -1.5$ Å, $y = -1.2$ Å, and $z = 1.25$ Å and a significantly smaller rotation κ of −2.9° about an axis with $\psi = 68.2°$ and $\phi = 148.8°$. The large κ value for reduced DsbA corresponds to an orientation in which the two domains of DsbA are more apart, thereby enlarging the wedge-shaped cleft between them.

To examine the different domain orientations further, we checked the angles between secondary structure elements of the two DsbA domains in the two structures. There is a cleft between the two domains which is formed on one hand by helix α1 and sheets β2 and β3 of the thioredoxin-like domain and on the other hand by helices α2 and α3 of the helical domain. We fitted cylinders to all secondary structure elements and subsequently determined the angles between these cylinders with the program MOLMOL (*83*). The results are summarized in Table 2. In general, the intradomain angle differences are small for monomers A and B of the crystal structure of oxidized DsbA (<3.0°), indicating that the structures of the individual domains are practically identical in both monomers. The differences in interdomain angles between the two monomers are also small (<3.7°). The structures of the individual domains are only slightly different in the structure of reduced DsbA as can be seen from the small differences in the intradomain angles between oxidized and reduced DsbA (<6.7°). The largest differences between the structures of the oxidized and reduced protein are observed for the interdomain angles. The absolute values of the angular differences are up to 20° between secondary structure elements from different domains, confirming that the cleft between the two DsbA domains is wider in the

FIGURE 3: (A, left) Ribbon drawing of the energy-minimized mean solution structure of reduced DsbA ($\langle SA \rangle_m$) showing the regular secondary structure and global fold of the protein. Secondary structure elements within the thioredoxin-like domain are colored in blue, and elements within the α-helical domain are colored in red. The N and C termini of DsbA as well as all secondary structure elements are indicated. The side chains of the two active site residues, Cys30 and Cys33, are shown explicitly with the S^{γ} and C^{β} atoms depicted as yellow and black spheres, respectively. The orientation of the DsbA molecule in this figure is referred to as the "standard orientation" and will be maintained in most figures of this paper. (B, right) Stereoview of the backbone atoms (N, C^{α}, C′, and O) of all residues for the family of 20 structures of reduced DsbA best fitted to N, C^{α}, and C′ atoms of the regions with regular secondary structure (residues 9−11, 22−25, 31−37, 42−48, 56−59, 68−82, 85−97, 105−114, 119−127, 130−144, 152−155, 159−161, and 171−185). This figure was produced with MOLMOL (*83*).

structure of the reduced protein. The simplest description of the different domain orientation is probably a comparison of the cleft's size in reduced and oxidized DsbA. In the crystal structure of oxidized DsbA, the cleft is roughly 14 Å long and varies in depth (5−12 Å) and width (8−11 Å). In the solution structure of the reduced protein, its size is considerably larger with a length of 20 Å, a depth of 5−10 Å, and a width of 10−14 Å.

Surface Features of Reduced DsbA. Several special surface features were identified in the crystal structure of oxidized DsbA which may be important for the interaction of DsbA with reduced unfolded polypeptides and other proteins (*13*, *41*). An extended hydrophobic patch and a hydrophobic groove incorporating a small hydrophobic pocket are located on one side of the DsbA molecule, close to the active site cysteines. In addition, an acidic patch is located in a second groove on the surface opposite to the active site. All these surface features are also present in the solution structure of reduced DsbA. Their general properties are the same, but their detailed location and size are slightly different in most of the cases (Figure 8).

The supposed peptide binding groove in oxidized DsbA is roughly 20 Å long, 10 Å wide, and 7 Å deep. It is formed exclusively from residues of the thioredoxin-like domain, i.e., Phe36 and Leu40 from helices α1 and α1′, Pro151 from the extended strand between helix α6 and strand β4, Gln160 from strand β5, and Pro163, Gln164, Thr168, Met171, Phe174, and Val175 from the flexible loop between strand β5 and the first turn of helix α7. The hydrophobic groove in reduced DsbA is formed by residues Phe36, Pro151, Gln160, Pro163, Gln164, Gly165, and Met166 and is shorter (17 Å) and not as wide (8−9 Å). This is mainly caused by the different conformation of the flexible loop between strand β5 and helix α7; the backbone of residues Gln164−Met166 and the side chain of Gln164 from this loop form an extended ridge at the lower edge of the groove that diminishes its width (Figure 8). The right end of the groove is formed by the side chain of Asp167 and the N terminus of helix α1 (residues Pro31 and His32), thus separating residues Leu40, Thr168, Met171, Phe174, and Val175 from the groove. At the left end of the groove, the side chain of Arg148 forms a flexible stalk that protrudes over the hydrophobic groove as well as over the incorporated hydrophobic pocket.

This hydrophobic pocket is located inside the hydrophobic groove, with dimensions of approximately 6 Å × 7 Å and 5 Å deep in oxidized DsbA. It is also formed exclusively by residues from the thioredoxin-like domain of DsbA: Phe36 and Ile42 from helices α1 and α1′, Pro151 from the active site, Met153 from strand β4, Leu161 from strand β5, and Tyr178 from the C-terminal helix α7. Glu24 is located below the pocket and contributes to a net negative charge within the pocket. In reduced DsbA, the hydrophobic pocket is also present and its dimensions are roughly the same, but it is formed by a slightly different set of amino acids: Met153 (which also participates in the oxidized protein) and Gln160 and Asn162 from strand β5. In addition, the entrance of the pocket is shielded by the side chain of Arg148 which forms a basic stalk that protrudes over it.

The hydrophobic patch, with an area of approximately 12 Å × 16 Å, is located near the active site cysteines of reduced DsbA. It is formed by residues from both DsbA domains: Phe29, just before the active site, Phe63−Gly66 from the first hinge region between the two domains, Leu68 from helix α2, and Val150 from an extended strand between helix α6

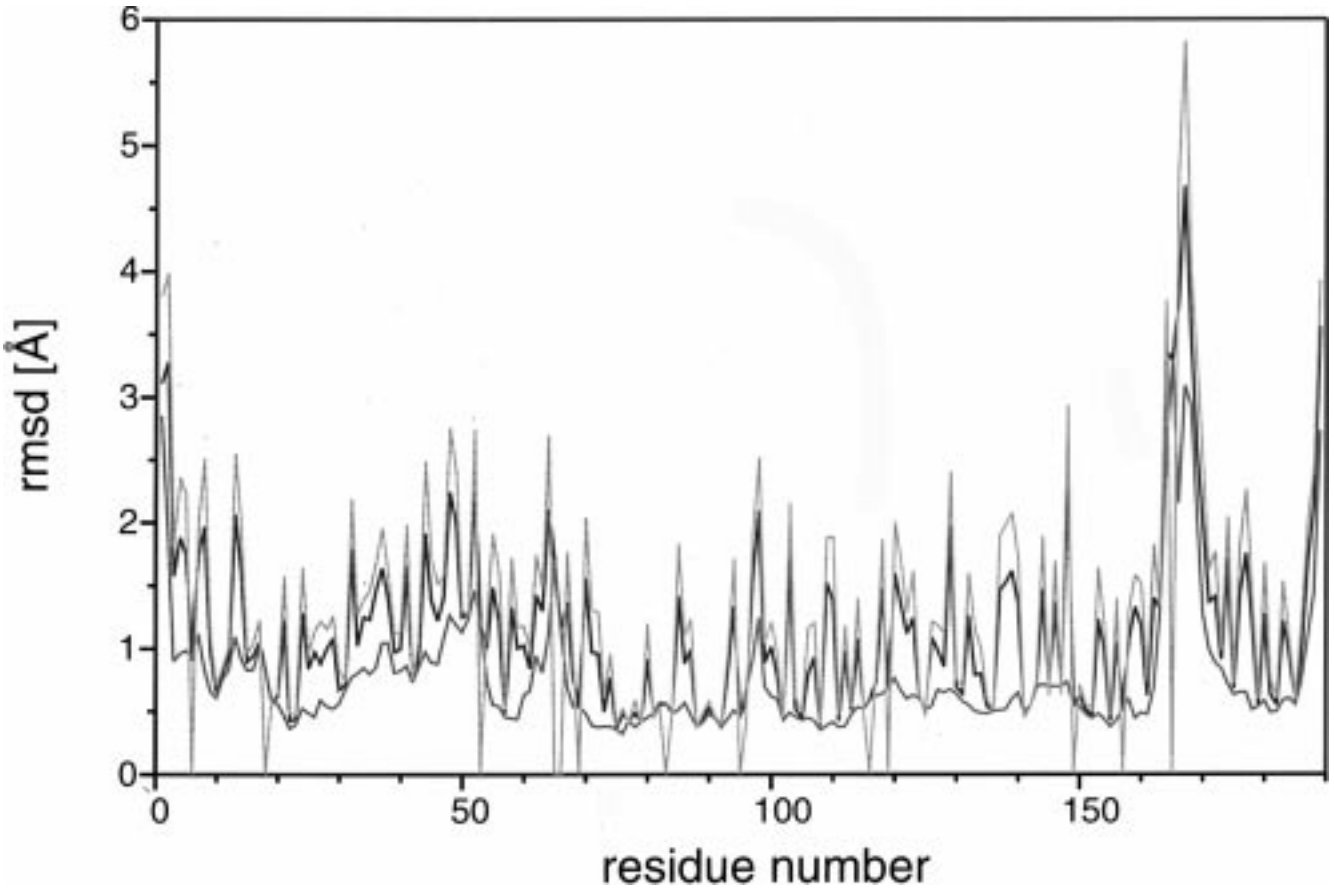

FIGURE 4: Residue-based root-mean-square deviations of the atomic coordinates among the SA structures from the energy-minimized mean structure for the backbone atoms N, C^{α}, C′, and O (red line), non-hydrogen side chain atoms (orange line), and all non-hydrogen atoms together (blue line).

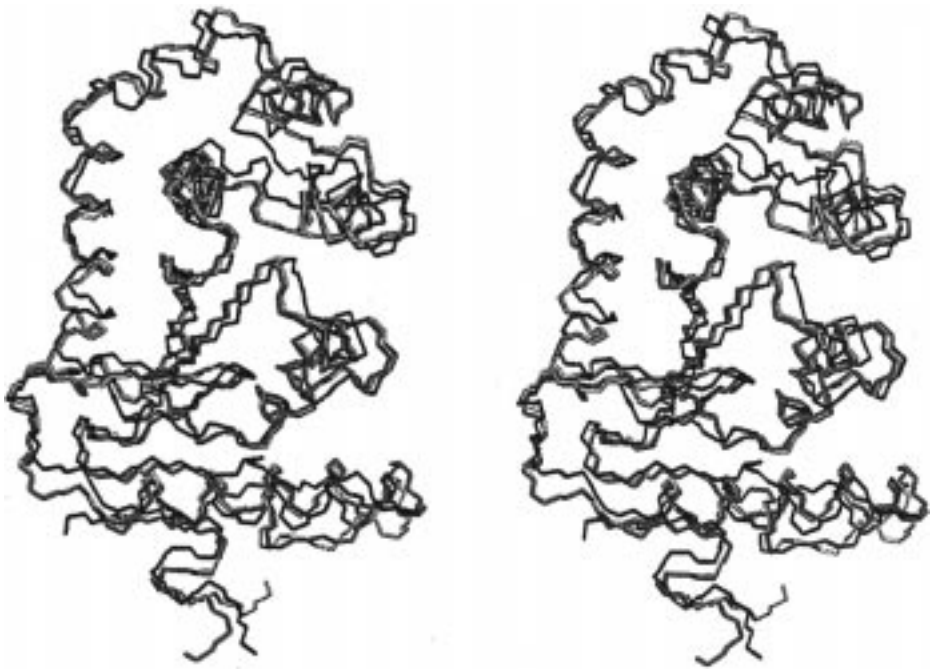

FIGURE 5: Stereoview of the backbone superposition of the energy-minimized mean solution structure of reduced DsbA (blue) with molecules A (red) and B (orange) from the asymmetric unit of the crystal structure of oxidized DsbA. The molecules were fitted to all N, C^{α}, and C′ atoms of the regions with regular secondary structure (residues 9−11, 22−25, 31−37, 42−48, 56−59, 68−82, 85−97, 105−114, 119−127, 130−144, 152−155, 159−161, and 171−185). This figure was produced with MOLMOL.

and strand β4. The same amino acids contribute to the hydrophobic patch in the structure of oxidized DsbA, and its size is basically similar.

In accordance with the structure of oxidized DsbA, the acidic patch is located in the wedge-shaped groove between the two domains at the face of the molecule just opposite

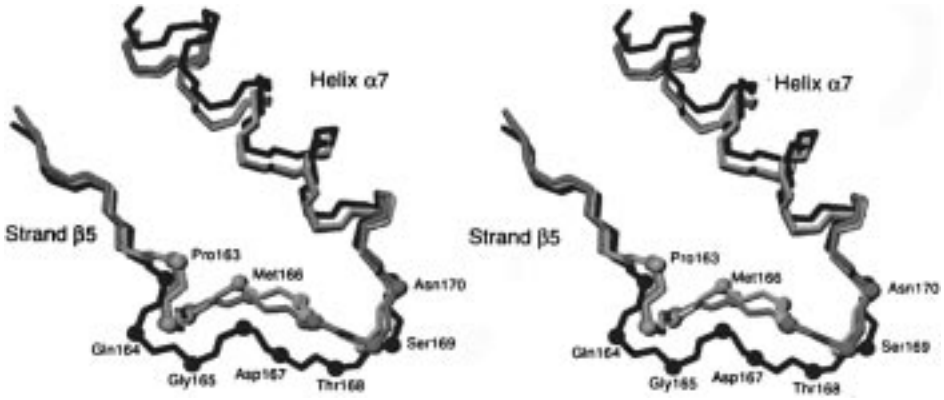

FIGURE 6: Detailed stereoview of the loop comprising residues 163−169 (located between strand β5 and helix α7), seen from the top of the molecule. Superposition of the backbone atoms of the energy-minimized mean solution structure of reduced DsbA (blue) with molecules A (red) and B (orange) from the asymmetric unit of the crystal structure of oxidized DsbA. C^{α} atoms within the loop are shown as small spheres with the corresponding residue depicted beneath. This figure was produced with MOLMOL.

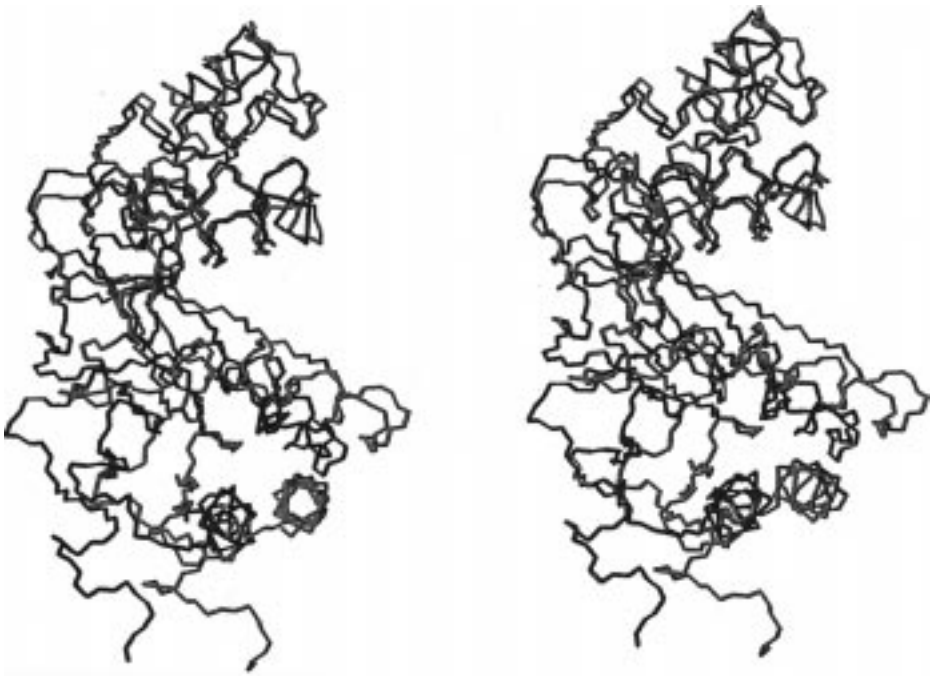

FIGURE 7: Backbone superposition of the energy-minimized mean solution structure of reduced DsbA (blue) with molecule A from the crystal structure of oxidized DsbA (red) in stereoview. Both molecules were fitted to the regular secondary structure elements of the α-helical domain of DsbA (all N, C^{α}, and C′ atoms of residues 68−82, 85−97, 105−114, and 119−127). The atoms of helix α6, which spans both domains of the protein, were excluded from the fit. The molecule is rotated by 90° to the left about the vertical axis with respect to the standard orientation. This figure was produced with MOLMOL.

the active site. The groove is formed by helices α1 and α1′ and strand β2 from the thioredoxin-like domain and by helices α2 and α3 from the helical domain of DsbA. The acidic patch itself is formed by the following six residues: Glu37, Glu38, and Asp44 from helices α1 and α1′ and Glu85, Asp86, and Glu94 from helix α3. In oxidized DsbA, the acidic patch is formed by the same amino acids but its area is smaller than that in the reduced protein. This is mainly a consequence of the different domain orientation. In the structure of reduced DsbA, the wedge-shaped cleft between the two domains has dimensions of approximately 20 Å (length) × 10−14 Å (width) × 5−10 Å (depth), thereby exposing more of the acidic patch. The solvent-exposed surface area of Glu37, Glu38, Asp44, and Glu94 is up to 20% larger in reduced DsbA than in the structure of the oxidized protein.

Active Site. Most NOE signals within the active site of DsbA are very weak. Therefore, some of the NOE patterns could not be unambiguously assigned. Despite these difficulties, the backbone conformation in the active site of reduced DsbA is well defined, but the side chain conformations are generally less precise. In particular, the conformation of the side chain of His32 is poorly defined, as well as the χ_1 angles of Phe29, Cys30, and Cys33. To visualize the local differences in the side chain conformations of residues 28−34, the energy-minimized mean solution structure of reduced DsbA and the two molecules from the crystal structure of oxidized DsbA were fitted onto the backbone atoms of residues Cys30−Cys33 (Figure 9). Most backbone conformations of residues 30−33 of reduced DsbA are nearly identical to their conformation in oxidized DsbA. The differences in the ϕ and ψ backbone angles of Pro31 and

Table 2: Comparison of Angles (in Degrees) between Regular Secondary Structure Elements from Both Domains of DsbA in the Crystal Structure of Oxidized DsbA and the Energy-Minimized Mean Solution Structure of Reduced DsbA

	oxidized DsbA			reduced DsbA		
	molecule A	molecule B	A−B[a]	mean NMR model	NMR-A[b]	NMR-B[c]
Intradomain Angles, Thioredoxin-like Domain						
$\beta2-\beta3$	23.6	23.4	0.2	22.5	−1.1	−0.9
$\alpha1-\beta2$	121.6	121.5	0.1	128.2	6.6	6.7
$\alpha1-\beta3$	143.4	146.4	3.0	144.5	1.1	−1.9
Intradomain Angles, Helical Domain						
$\alpha2-\alpha3$	160.3	159.3	1.0	153.9	−6.4	−5.4
$\alpha2-\alpha4$	26.1	24.0	2.1	22.6	−3.5	−1.4
$\alpha3-\alpha4$	134.6	135.9	1.3	133.0	−1.6	−2.9
Interdomain Angles between the Two Domains						
$\alpha1-\alpha2$	30.4	27.5	2.9	16.8	−13.6	−10.7
$\alpha1-\alpha3$	130.4	132.7	2.3	138.7	8.3	6.0
$\alpha1-\alpha4$	4.3	3.8	0.5	20.3	16.0	16.5
$\beta2-\alpha2$	139.2	137.6	1.6	126.7	−12.5	−10.9
$\beta2-\alpha3$	31.8	30.0	1.8	49.0	17.2	19.0
$\beta2-\alpha4$	124.2	122.9	1.3	108.5	−15.7	−14.4
$\beta3-\alpha2$	148.9	145.4	3.5	135.8	−13.1	−9.6
$\beta3-\alpha3$	36.0	35.9	0.1	52.8	16.8	16.9
$\beta3-\alpha4$	145.2	141.5	3.7	124.2	−21.0	−17.3

[a] Difference between molecule A and B in the crystal structure of oxidized DsbA. [b] Difference between the energy-minimized mean solution structure of reduced DsbA and molecule A in the crystal structure of oxidized DsbA. [c] Difference between the energy-minimized mean solution structure of reduced DsbA and molecule B in the crystal structure of oxidized DsbA.

His32 compared to those of oxidized DsbA are smaller than 15°. However, the backbone angles for Cys30 and Cys33 are different from those of the oxidized protein so that the backbone starts to deviate before Cys30 and after Cys33. The most prominent local difference in the active site loop is the tilting of the ring of Pro31 by about 20° toward the inside of the active site as a consequence of the different ψ angle of Cys30. Another difference is the orientation of the Cys30 $C^{\alpha}-C^{\beta}$ bond. With respect to oxidized DsbA, it is turned by about 30° more in the direction of Pro31 and to the outside of the loop formed by residues 27−32. The side chain of His32 is largely disordered in χ_1, but in the majority of the structures, it clusters between the same two conformations present in oxidized DsbA (A, $\chi_1 = -$sc; and B, $\chi_1 =$ ap). The side chain conformation of Cys33 also differs from that in oxidized DsbA as a consequence of the different Cys33 ϕ and ψ angles; the $C^{\alpha}-C^{\beta}$ bond is rotated clockwise by about 30° around the axis of helix α1. The first loop of the active site helix resembles more a 3^{10}-helix than an α-helix in oxidized DsbA. The 3^{10}-helix character is even more pronounced in the reduced protein.

DISCUSSION

Comparison of the Solution Structure of Reduced DsbA and the Crystal Structure of Oxidized DsbA. The low rmsd among the NMR models of DsbA allows an analysis of the structural differences between the solution structure of reduced DsbA and the crystal structure of oxidized DsbA (*12*, *13*). Overall, the structures of oxidized and reduced DsbA are very similar, but the local differences between the structures of both redox forms are more pronounced compared to *E. coli* thioredoxin (*45*), human thioredoxin (*37*, *39*), and *E. coli* glutaredoxin (*47*). Most of the local differences in main chain conformation occur at both termini of the protein and in loop regions at the protein surface. They may reflect crystal packing effects and the inherent mobility of solvent-exposed regions. A good example is the region between residues 163 and 174 which is located directly after strand $\beta5$ and forms a mobile loop (residues 163−169) and the first turn of helix α7 (residues 170−174). This stretch adopts different conformations in the ensemble of NMR structures when compared to the X-ray model (Figure 6), and its rmsd values are the highest among the NMR models. These deviations are most likely an inherent feature of the loop's flexibility and lead to a different average conformation when comparing the solution structure with the crystal structure. Indeed, preliminary relaxation measurements (unpublished results) and increased *B*-factors for residues 163−169 in the crystal structure of oxidized DsbA point to a higher flexibility of this segment in both redox states. Another reason for the structural difference could be crystal contacts between the two monomers in the asymmetric unit of the crystal structure involving residues 163−174, which also lead to different conformations of this region in both monomers of oxidized DsbA. Residues 163−174 have been postulated to be important for the interaction with polypeptide substrates (*13*). Its flexibility may thus be an intrinsic

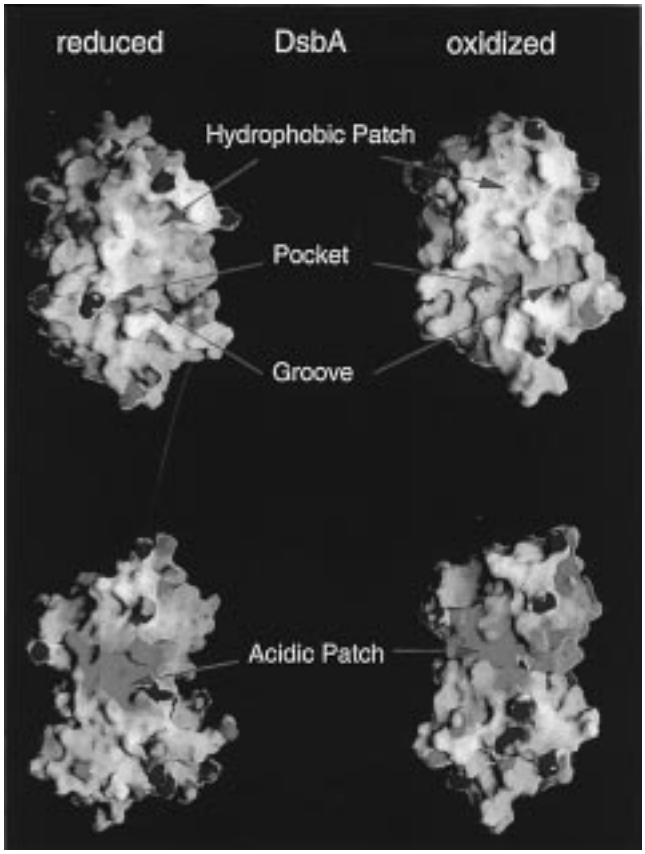

FIGURE 8: Electrostatic surfaces of the energy-minimized mean solution structure of reduced DsbA (left) and monomer A from the crystal structure of oxidized DsbA (right) generated with GRASP (*91*). Surfaces are colored by charge (red is negative, blue is positive, and white is uncharged or hydrophobic). The γ-sulfur atom of Cys30 is depicted as a yellow sphere. The hydrophobic pocket and groove as well as the acidic patch of the molecule are denoted by arrows. The top orientation of the molecule is the same as the standard orientation. The lower molecules are rotated 180° about a vertical axis.

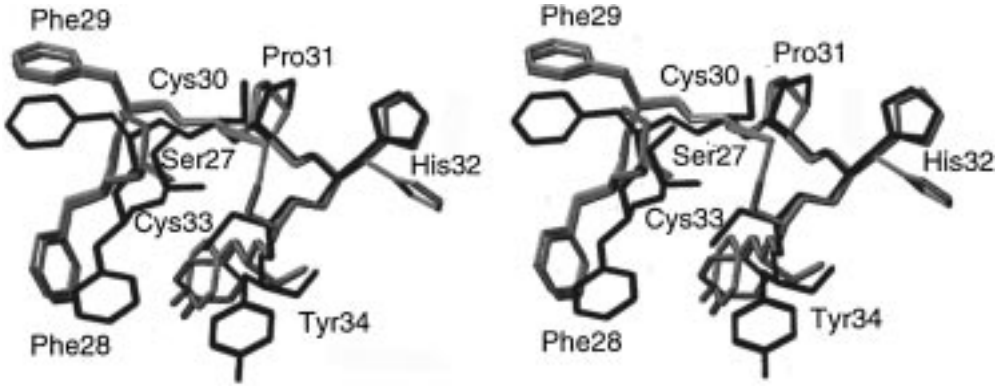

FIGURE 9: Detailed stereoview of the active site of DsbA. The backbone and heavy side chain atoms of residues 28−34 are shown for the energy-minimized mean solution structure of reduced DsbA (blue) and molecules A (red) and B (orange) from the asymmetric unit of the crystal structure of oxidized DsbA. The structures were fitted to the backbone atoms (N, C^{α}, and C′) of residues 30−33 (active site residues). This figure was produced with MOLMOL.

property reflecting the function of DsbA, especially since a conformational difference in this loop affects the size of the hydrophobic groove (see below).

Conformational Differences within the Active Site and Stabilization of the Cys30 Thiolate Anion. The structural differences in the active site between reduced and oxidized DsbA are very subtle. All NOE signals present in the region of the active site residues were examined very carefully. Unfortunately, not many active site NOEs could be included in structure calculations since a considerable number of resonances could not be assigned. Therefore, the precision of the active site region in the structures of reduced DsbA is not as good as in other parts of the protein, and statements about structural differences in this region are generally not as certain as those for the rest of the protein. As an example, the side chain conformation of His32 is largely disordered in the structural family with χ_1 angles distributed between the −sc and ap conformations. The NOE intensity pattern between the H^{α} and H^{β} resonances indicates either a +sc dihedral angle or a 1:1 equilibrium between the −sc and ap conformations. Since the H^N proton of His32 could not be assigned, any information about H^N-H^{β} NOE intensities or from the HNHB spectrum is missing, and one cannot distinguish between these two possibilities.

In the crystal structure of oxidized DsbA, the His32 side chain has two different conformations. In monomer A, it has a −sc conformation, although rotation around the $C^{\alpha}-C^{\beta}$ bond is generally unrestricted. In monomer B, the conformation is ap. The −sc conformation is forbidden due to a steric clash with the backbone of the other monomer, and the ap conformation is furthermore stabilized by crystal contacts, e.g., a hydrogen bond between H^{δ}(His32B) and O′-(Lys98A). Thus, it seems that His32 can adopt both conformations in both redox states of DsbA and that the best interpretation of the NMR data is a conformational heterogeneity between the −sc and ap conformations, which is also yielded by the structure calculations.

The thiolate anion of Cys30 is populated to at least 60% at pH 3.7. Nevertheless, the structure of the active site region in reduced DsbA reveals no unequivocal hint about the factors that stabilize the thiolate and cause the low pK_a value of the Cys30 thiol. The network of charged residues Glu24, Lys58, Glu37, and Glu38 in the vicinity of the active site is basically the same compared to the crystal structure of oxidized DsbA. This is consistent with site-directed mutagenesis experiments which proved that none of these residues is responsible for the low pK_a of Cys30 (*84*). The only interaction of the Cys30 thiolate with an amino acid side chain seems to be with His32, whose replacement by several uncharged residues increased the Cys30 pK_a by 0.3−1.5 units (*21*, *85*). Very similar observations were reported for the exchange of the equivalent histidine in the catalytic domain of PDI (*33*) and *E. coli* thioredoxin (*35*). Another possible reason for the stabilization of the Cys30 thiolate would be a charged hydrogen bond with either the S^{γ} or the H^N proton of Cys33 (*18*, *29*, *38*, *43*). As for the hypothesis of a shared proton between the sulfur atoms of Cys30 and Cys33, no clear statement can be derived from the NMR data since the side chain conformations of both residues are not well defined in the NMR models. Depending on the χ_1 conformation of Cys30 and Cys33, the closest possible distance between the S^{γ} atoms of the two cysteines is smaller than the covalent distance of 2 Å, and the largest possible distance is 7 Å. If the side chain conformation is the same in both redox states, the distance would be 3.7 Å. Thus, the possibility of a shared proton between the S^{γ} atoms of Cys30 and Cys33 cannot be excluded in this NMR model, but it appears unlikely since the pK_a of Cys30 is not significantly affected in the DsbA variant Cys33Ala (M. Huber-Wunderlich and R. Glockshuber, unpublished results). The same holds true for a hypothetical shared proton between S^{γ}(Cys30) and H^N(Cys33). The distance between the two atoms varies between the covalent distance and 4.5 Å, depending on the χ_1 conformation of Cys30. Regarding all these arguments, we believe that the most probable reason for the stabilization of the Cys30 thiolate is its favorable electrostatic interaction with the helix dipole of the active site α-helix (*26*, *30*). In accordance, the pK_a of the nucleophilic thiolate has been shown to be extremely sensitive to amino acid replacements within the active site helix and in particular to exchanges of the Xaa-Xaa dipeptide between the catalytic cysteines (*21*, *23*, *31*−*35*). In the case of DsbA, certain Xaa-Xaa mutations increase the pK_a of Cys30 by more than 3 units (*21*, *31*).

Domain Orientation. The orientation of the two domains of DsbA is different in the reduced protein when compared to the crystal structure of oxidized DsbA. Superposition of the backbone of the mean solution structure of reduced DsbA with the thioredoxin-like domain of molecule A of the crystal structure of oxidized DsbA yielded a different orientation

compared to fitting of the molecule to the helical domain of molecule A of the crystal structure (Figure 7). This difference corresponds to a wider cleft between the two domains in reduced DsbA compared to that in the oxidized protein. The angle of this wedge-shaped cleft, which is formed by helices α2 and α3 from the helical domain and by helix α1 and sheets β2 and β3 from the thioredoxin-like domain of DsbA, is increased by about 10−20°. This is, in fact, the largest difference between the solution structure of reduced DsbA and the crystal structure of oxidized DsbA. If the observed different domain orientation was a consequence of the reduction, the structural difference between both redox forms of DsbA would be larger compared to that reported for the one-domain thiol−disulfide oxidoreductases thioredoxin and glutaredoxin, which undergo only minor structural changes upon reduction of the active site disulfide bond (*29*, *37*, *39*, *42*−*47*).

The relative orientation of the two domains in the solution structure is exclusively defined by experimental NMR constraints. The nonbonded terms of the energy function in X-PLOR are represented by a van der Waals repulsion term, and no Lennard-Jones, electrostatic, or hydrogen bonding terms were used in the NMR structure calculations (*86*, *87*). The density of NOEs at the domain interface is equal to the density within the domains. However, NOE signals between protons in the cleft that should be present on the basis of the crystal structure of oxidized DsbA (if one assumes that the domain arrangement in reduced DsbA is the same as in the crystal structure of oxidized DsbA) are unambiguously absent in the NOESY spectra up to mixing times of 200 ms. Additionally, the value of angular difference is too large to be solely an effect of missing NOEs. The error in the rotation angle κ was estimated with X-PLOR to be ±8°. This is considerably smaller than the total rotation of the domains of $\kappa = 20°$, confirming the significance of the structural difference. Analogous observations regarding the orientation of one subunit with respect to another have been made for the solution and crystal structures of interleukin-8 (*86*). The solution structure of reduced DsbA and the crystal structure of the oxidized protein were however obtained under different conditions. In particular, the pH used for crystallization of oxidized DsbA was 6.5 (*88*), whereas the solution structure was determined at pH 3.7. In addition, the algorithms used for structure calculations were different. To rule out possible influences of these factors on the comparison of the two forms of DsbA, we are presently also determining the solution structure of oxidized DsbA by NMR spectroscopy under identical conditions (see below).

Analysis of Differences between the NMR Spectra of Reduced and Oxidized DsbA at pH 3.7 and 300 K. The ^{1}H, ^{15}N, and $^{13}C^{\alpha}$ chemical shifts of the backbone resonances are highly sensitive markers for local conformational and electronic changes. We have completed the sequential assignment of the backbone resonances of oxidized DsbA at pH 3.7 and 300 K, which allows the analysis of chemical shift differences caused by the different redox states of the enzyme. The ^{1}H, ^{15}N, and $^{13}C^{\alpha}$ shifts are in general identical within fractions of parts per million for reduced and oxidized DsbA, except for the region around the active site (Figure 10). Thus, as expected, the overall structure of the two redox forms at pH 3.7 is very similar, and the largest differences

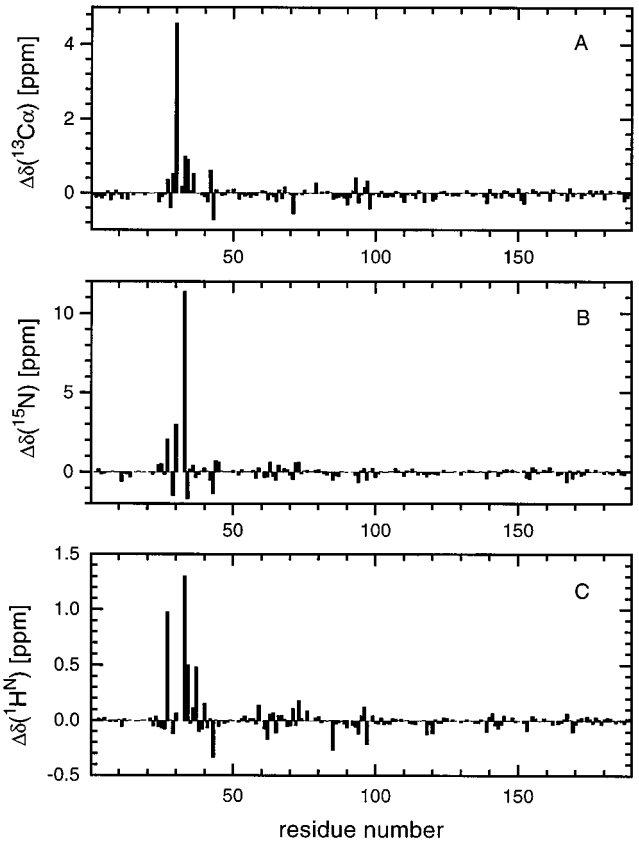

FIGURE 10: Differences of chemical shifts between reduced and oxidized DsbA at pH 3.7 and 300 K plotted against the residue number: (A) shift differences for $^{13}C^{\alpha}$ resonances, (B) shift differences for ^{15}N backbone resonances, and (C) shift differences for $^{1}H^{N}$ backbone resonances. The differences in chemical shifts are generally very small except for residues in vicinity of the active site of DsbA.

in structure, and especially in charge distribution, occur in the active site of DsbA. Cys30 shows the largest $^{13}C^{\alpha}$ shift difference, whereas its change in ^{1}H and ^{15}N shifts is not so pronounced. This can be expected since the conformation of Cys30 is basically the same in oxidized and reduced DsbA. However, the Cys30 thiolate anion is populated to 60% at pH 3.7. The negative charge should shift the C^{α} resonance downfield, as is indeed observed. The largest difference in ^{1}H and ^{15}N shifts is observed for Cys33, possibly reflecting different conformations of this residue in both redox states at pH 3.7 in solution. However, the data for Cys30 and Cys33 have to be considered with care since the "random coil" chemical shifts of cysteine residues in the disulfide, thiol, and thiolate forms are different, at least for ^{13}C (*89*). Apart from the two active site cysteines, large chemical shift differences are also observed for other residues close to the active site, namely, Ser27, Phe29, Tyr34, Glu37, and Ser43 (Figure 10).

Implications of Structural Differences for the Reaction Cycle of DsbA. The most prominent differences between the structures of oxidized and reduced DsbA are the distinct orientations of the two domains. Together with the different conformations of the loop between sheet β5 and helix α7, the different domain orientations alter some surface features of DsbA. If these structural differences are exclusively a consequence of the different redox states, they might play an important role in the reaction cycle of DsbA which consists of the following steps: binding of an unfolded,

reduced polypeptide by oxidized DsbA, oxidation and subsequent release of the polypeptide, binding and reoxidation of DsbA by DsbB, and subsequent dissociation of the DsbA−DsbB complex. It has been suggested that the hydrophobic surface features surrounding the active site disulfide are important for the binding of unfolded peptides to oxidized DsbA and that the acidic patch, located in the cleft at the opposite side of the protein, might be a binding site for DsbB (*13*). Our observations are consistent with this suggestion. The hydrophobic groove is shorter and narrower in the solution structure of reduced DsbA; the associated hydrophobic pocket has a different location, and its entrance is partially blocked. Thus, the structural differences in the hydrophobic groove and the hydrophobic pocket should make binding of a peptide to DsbA more unfavorable. In addition, the different domain orientation in reduced DsbA may improve the accessibility of the acidic patch and possibly enhance the binding to DsbB. The supposed lowered affinity of reduced DsbA for unfolded polypeptides would also be in agreement with the fact that the enzyme is a very efficient oxidant but possesses a relatively weak disulfide isomerase activity (*4*, *6*, *17*, *25*). Thus, it appears that the observed differences between the crystal structure of oxidized DsbA and the solution structure of reduced DsbA are in good agreement with the functional requirements for the enzyme's catalytic efficiency in vivo.

During preparation of this paper, we have learned that a crystal structure of reduced DsbA has been determined to 2.7 Å resolution (J. Martin, personal communication) and that this structure is more similar to the crystal structure of oxidized DsbA than to the solution structure of reduced DsbA. Whether the differences between the solution and crystal structures of reduced DsbA are caused by different pH conditions, crystal packing effects, influences of the refinement protocols, or other reasons cannot be decided at this time, and future details will have to await an extensive analysis of the two structures determined by both NMR spectroscopy and X-ray crystallography.

ACKNOWLEDGMENT

We thank Peter Güntert, Jenny Martin, Ekkehard Mössner, and Stefan Strobl for helpful discussions and Jens Fricke, Ralph Gauges, Silke Jonda, Thomas Kast, and Florian Kreppel for their help during the assignment of resonances and extraction of distance constraints.

SUPPORTING INFORMATION AVAILABLE

A figure showing a strip plot from HNCA, CBCA(CO)-NH, and CBCANH spectra, a rmsd plot of the torsion angles versus the amino acid sequence, a plot of the number of NOE constraints versus the amino acid sequence, Ramachandran plots for the family of 20 structures and for the energy-minimized mean structure of reduced DsbA, and a sausage plot showing the definition of the structures as the diameter of a spline curve through the protein's backbone (8 pages). Ordering information is given on any current masthead page. In addition to the material available from *Biochemistry*, a table with the ^{1}H, ^{13}C, and ^{15}N chemical shifts of reduced DsbA is available from the authors upon request and will be deposited with the BioMagResBank.

REFERENCES

1. Jaenicke, R. (1993) *Curr. Opin. Struct. Biol. 3*, 104−112.
2. Bardwell, J. C. A., McGovern, K., and Beckwith, J. (1991) *Cell 67*, 581−589.
3. Kamitani, S., Akiyama, Y., and Ito, K. (1992) *EMBO J. 11*, 57−62.
4. Wunderlich, M., Otto, A., Seckler, R., and Glockshuber, R. (1993) *Biochemistry 32*, 12251−12256.
5. Darby, N. J., and Creighton, T. E. (1994) *Biochemistry 33*, 5205−5211.
6. Darby, N. J., and Creighton, T. E. (1995) *Biochemistry 34*, 3576−3587.
7. Bardwell, J. C. A., Lee, J.-O., Jander, G., Martin, N., Belin, D., and Beckwith, J. (1993) *Proc. Natl. Acad. Sci. U.S.A. 90*, 1038−1042.
8. Jander, G., Martin, N. L., and Beckwith, J. (1994) *EMBO J. 13*, 5121−5127.
9. Kishigami, S., Kanaya, E., Kikuchi, M., and Ito, K. (1995) *J. Biol. Chem. 270*, 17072−17074.
10. Guilhot, C., Jander, G., Martin, N. L., and Beckwith, J. (1995) *Proc. Natl. Acad. Sci. U.S.A. 92*, 9895−9899.
11. Kishigami, S., and Ito, K. (1996) *Genes Cells 1*, 201−208.
12. Martin, J. L., Bardwell, J. C. A., and Kuriyan, J. (1993) *Nature 365*, 464−468.
13. Guddat, L. W., Bardwell, J. C. A., Zander, T., and Martin, J. L. (1997) *Protein Sci. 6*, 1148−1156.
14. Martin, J. L. (1995) *Structure 3*, 245−250.
15. Zapun, A., Bardwell, J. C. A., and Creighton, T. E. (1993) *Biochemistry 32*, 5083−5092.
16. Zapun, A., Cooper, L., and Creighton, T. E. (1994) *Biochemistry 33*, 1907−1914.
17. Wunderlich, M., Otto, A., Maskos, K., Mücke, M., Seckler, R., and Glockshuber, R. (1995) *J. Mol. Biol. 247*, 28−33.
18. Katti, S. K., Robbins, A. J., Yang, Y., and Wells, W. W. (1995) *Protein Sci. 4*, 1998−2005.
19. Kemmink, J., Darby, N. L., Dijkstra, K., Scheek, R. M., and Creighton, T. E. (1995) *Protein Sci. 4*, 2587−2593.
20. Wunderlich, M., and Glockshuber, R. (1993) *Protein Sci. 2*, 717−726.
21. Huber-Wunderlich, M., and Glockshuber, R. (1998) *Folding Des. 3*, 161−171.
22. Lin, T. Y., and Kim, P. S. (1989) *Biochemistry 28*, 5282−5287.
23. Krause, G., Lundström, J., Barca, J. L., Pueyo de la Costa, C., and Holmgren, A. (1991) *J. Biol. Chem. 266*, 9494−9500.
24. Wunderlich, M., Jaenicke, R., and Glockshuber, R. (1993) *J. Mol. Biol. 233*, 559−566.
25. Zapun, A., and Creighton, T. E. (1994) *Biochemistry 33*, 5202−5211.
26. Nelson, J. W., and Creighton, T. E. (1994) *Biochemistry 33*, 5974−5983.
27. Frech, C., Wunderlich, M., Glockshuber, R., and Schmid, F. X. (1996) *EMBO J. 15*, 392−398.
28. Hol, W. G. J. (1985) *Prog. Biophys. Mol. Biol. 45*, 149−195.
29. Katti, S. K., LeMaster, D. M., and Eklund, H. (1990) *J. Mol. Biol. 212*, 167−184.
30. Kortemme, T., and Creighton, T. E. (1995) *J. Mol. Biol. 253*, 799−812.
31. Grauschopf, U., Winther, J. R., Korber, P., Zander, T., Dallinger, P., and Bardwell, J. C. A. (1995) *Cell 83*, 947−955.
32. Chivers, P. T., Laboissière, M. C. A., and Raines, T. (1996) *EMBO J. 15*, 2659−2667.
33. Kortemme, T., Darby, N. J., and Creighton, T. E. (1996) *Biochemistry 35*, 14503−14511.
34. Rossmann, R., Stern, D., Loferer, H., Jacobi, A., Glockshuber, R., and Hennecke, H. (1997) *FEBS Lett. 406*, 249−254.
35. Mössner, E., Huber-Wunderlich, M., and Glockshuber, R. (1998) *Protein Sci.* (in press).
36. Forman-Kay, J. D., Clore, G. M., and Gronenborn, A. M. (1992) *Biochemistry 31*, 3442−3452.
37. Qin, J., Clore, G. M., and Gronenborn, A. M. (1994) *Structure 2*, 503−522.
38. Jeng, M.-F., Holmgren, A., and Dyson, H. J. (1995) *Biochemistry 34*, 10101−10105.

39. Weichsel, A., Gasdaska, J. R., Powis, G., and Montfort, W. R. (1996) *Structure 4*, 735−751.
40. Warwicker, J., and Gane, P. J. (1996) *FEBS Lett. 385*, 105−108.
41. Hu, S.-H., Peek, J. A., Rattigan, E., Taylor, R. K., and Martin, J. L. (1997) *J. Mol. Biol. 268*, 137−146.
42. Dyson, H. J., Gippert, G. P., Case, D. A., Holmgren, A., and Wright, P. E. (1990) *Biochemistry 29*, 4129−4136.
43. Forman-Kay, J. D., Clore, G. M., Wingfield, P. T., and Gronenborn, A. M. (1991) *Biochemistry 30*, 2685−2698.
44. Eklund, H., Ingelman, M., Söderberg, B.-O., Uhlin, T., Nordlund, P., Nikkola, M., Sonnerstam, U., Joelson, T., and Petratos, K. (1992) *J. Mol. Biol. 228*, 596−618.
45. Jeng, M.-F., Campbell, A. P., Begley, T., Holmgren, A., Case, D. A., Wright, P. E., and Dyson, H. J. (1994) *Structure 2*, 853−868.
46. Sodano, P., Xia, T. H., Bushweller, J. H., Björnberg, O., Holmgren, A., Billeter, M., and Wüthrich, K. (1991) *J. Mol. Biol. 221*, 1311−1324.
47. Xia, T.-H., Bushweller, J. H., Sodano, P., Billeter, M., Björnberg, O., Holmgren, A., and Wüthrich, K. (1992) *Protein Sci. 1*, 310−321.
48. Studier, F. W., and Moffatt, B. A. (1986) *J. Mol. Biol. 189*, 113−130.
49. Strobl, S., Mühlhahn, P., Bernstein, R., Wiltscheck, R., Maskos, K., Wunderlich, M., Huber, R., Glockshuber, R., and Holak, T. A. (1995) *Biochemistry 34*, 8281−8293.
50. Sambrook, J., Fritsch, E. F., and Maniatis, T. (1989) *Molecular Cloning: A Laboratory Manual*, 2nd ed., Cold Spring Harbor Laboratory Press, Cold Spring Harbor, NY.
51. Griffey, R. H., and Redfield, A. G. (1985) *Biochemistry 24*, 817−822.
52. Riesenberg, D., Menzel, K., Schulz, V., Schumann, K., Veith, G., Zuber, G., and Knorre, W. A. (1990) *Appl. Microbiol. Biotechnol. 34*, 77−82.
53. Marion, D., and Wüthrich, K. (1983) *Biochem. Biophys. Res. Commun. 113*, 967−974.
54. Marion, D., Driscoll, P. C., Kay, L. E., Wingfield, P. T., Bax, A., Gronenborn, A., and Clore, G. M. (1989) *Biochemistry 28*, 6150−6156.
55. Plateau, P., and Gueron, M. (1982) *J. Am. Chem. Soc. 104*, 7310−7311.
56. Sklenar, V., Piotto, M., Leppik, R., and Saudek, V. (1993) *J. Magn. Reson., Ser. A 102*, 241−245.
57. Levitt, M. H., Freeman, R., and Frenkiel, T. (1982) *J. Magn. Reson. 50*, 345−348.
58. Gueron, M., Plateau, P., and Decorps, M. (1991) *Prog. Nucl. Magn. Reson. Spectrosc. 23*, 135−209.
59. Zuiderweg, E. R. P., and Fesik, S. W. (1989) *Biochemistry 28*, 2387−2391.
60. Marion, D., Ikura, M., Tschudin, R., and Bax, A. (1989) *J. Magn. Reson. 85*, 393−399.
61. Mori, S., Abeyguna Wardana, C., O'Neil Johnson, M., and van Zijl, P. C. M. (1995) *J. Magn. Reson., Ser. B 108*, 94−98.
62. Grzesiek, S., and Bax, A. (1992) *J. Magn. Reson. 96*, 432−440.
63. Clubb, R. T., Thanabal, V., and Wagner, G. (1992) *J. Magn. Reson. 97*, 213−217.
64. Muhandiram, D. R., and Kay, L. E. (1994) *J. Magn. Reson., Ser. B 103*, 203−216.
65. Grzesiek, S., and Bax, A. (1992) *J. Magn. Reson. 99*, 201−207.
66. Grzesiek, S., and Bax, A. (1993) *J. Biomol. NMR 3*, 185−204.
67. Wang, A. C., Lodi, P. J., Qin, J., Vuister, G. W., Gronenborn, A. M., and Clore, G. M. (1994) *J. Magn. Reson., Ser. B 105*, 196−198.
68. Vuister, G. W., and Bax, A. (1993) *J. Am. Chem. Soc. 115*, 7772−7777.
69. Archer, S. J., Ikura, M., Torchia, D. A., and Bax, A. (1991) *J. Magn. Reson. 95*, 636−641.
70. Powers, R., Gronenborn, A. M., Clore, G. M., and Bax, A. (1991) *J. Magn. Reson. 94*, 209−213.
71. Kay, L. E., Xu, G.-Y., Singer, A. U., Muhandiram, D. R., and Forman-Kay, J. D. (1993) *J. Magn. Reson., Ser. B 101*, 333−337.
72. Shaka, A. J., Lee, C. J., and Pines, A. (1988) *J. Magn. Reson. 77*, 274−293.
73. Muhandiram, D. R., Farrow, N., Xu, G. Y., Smallcombe, S. J., and Kay, L. E. (1993) *J. Magn. Reson., Ser. B 102*, 317−321.
74. Jeener, J., Meier, B. H., Bachmann, P., and Ernst, R. R. (1979) *J. Chem. Phys. 71*, 4546−4553.
75. Cieslar, C., Ross, A., Zink, T., and Holak, T. A. (1993) *J. Magn. Reson., Ser. B 101*, 97−101.
76. Cavanagh, J., Fairbrother, W. J., Palmer, A. G., III, and Skelton, N. J. (1996) *Protein NMR Spectroscopy*, Acadamic Press, San Diego, CA.
77. Bernstein, R., Cieslar, C., Ross, A., Oschkinat, H., Freund, J., and Holak, T. A. (1993) *J. Biomol. NMR 3*, 245−251.
78. Wagner, G., Braun, W., Havel, T. F., Schaumann, T., Go, N., and Wüthrich, K. (1987) *J. Mol. Biol. 196*, 611−639.
79. Hyberts, S. G., Mäki, W., and Wagner, G. (1987) *Eur. J. Biochem. 164*, 625−635.
80. Holak, T. A., Gondol, D., Otlewski, J., and Wilusz, T. (1989) *J. Mol. Biol. 210*, 635−648.
81. Wüthrich, K. (1986) *NMR of Proteins and Nucleic Acids*, Wiley, New York.
82. Brünger, A. T. (1993) *X-PLOR Version 3.1 Manual*, Yale University Press, New Haven, CT.
83. Koradi, R., Billeter, M., and Wüthrich, K. (1996) *J. Mol. Graphics 14*, 51−55.
84. Jacobi, A., Huber-Wunderlich, M., Hennecke, J., and Glockshuber, R. (1997) *J. Biol. Chem. 272*, 21692−21699.
85. Guddat, L. W., Bardwell, J. C. A., Glockshuber, R., Huber-Wunderlich, M., Zander, T., and Martin, J. L. (1997) *Protein Sci. 6*, 1893−1900.
86. Clore, G. M., and Gronenborn, A. M. (1991) *J. Mol. Biol. 217*, 611−620.
87. Nilges, M., Clore, G. M., and Gronenborn, A. M. (1988) *FEBS Lett. 229*, 317−324.
88. Martin, J. L., Waksman, G., Bardwell, J. C. A., Beckwith, J., and Kuriyan, J. (1993) *J. Mol. Biol. 230*, 1097−1100.
89. Howarth, O. W., and Lilley, D. M. J. (1978) *Prog. NMR Spectrosc. 12*, 1−40.
90. Wishart, D. S., Sykes, B. D., and Richards, F. M. (1991) *J. Mol. Biol. 222*, 311−333.
91. Nicholls, A., Bharadwaj, R., and Honig, B. (1993) *Biophys. J. 64*, A116.

BI980136Y